Analyst

Accepted Manuscript

This article can be cited before page numbers have been issued, to do this please use: H. Zhu, F. Lu, X. Wu and J. Zhu, *Analyst*, 2015, DOI: 10.1039/C5AN01634G.

ROYAL SOCIETY OF CHEMISTRY

www.rsc.org/analyst

Cite this: DOI: 10.1039/c0xx00000x

www.rsc.org/xxxxxx

View Article Online
DOI: 10.1039/C5AN01634G

ARTICLE TYPE

An Upconversion Fluorescent Resonant Energy Transfer Biosensor for Hepatitis B Virus (HBV) DNA Hybridization Detection†

Hao Zhu, ‡ Feng Lu,‡ Xing-Cai Wu,* and Jun-Jie Zhu*

Received (in XXX, XXX) Xth XXXXXXXXX 20XX, Accepted Xth XXXXXXXXX 20XX
DOI: 10.1039/b000000x

A novel fluorescent resonant energy transfer (FRET) biosensor was fabricated for the detection of hepatitis B virus (HBV) DNA using poly(ethylenimine) (PEI) modified upconversion nanoparticles (NH_2-UCNPs) as energy donor and gold nanoparticles (Au NPs) as acceptor. The PEI modified upconversion nanoparticles were prepared directly with a simple one-pot hydrothermal method, which provides high quality amino-group functionalized UCNPs with uniform morphology and strong upconversion luminescence. Two single-stranded DNA, which were partially complementary to each other, were then conjugated with NH_2-UCNPs and Au NPs, respectively. When DNA conjugated NH_2-UCNPs and Au NPs were mixed together, the hybridization between complementary DNA sequence on UCNPs and Au NPs will lead to the quench of the upconversion luminescence due to the FRET process. Meanwhile, upon the addition of target DNA, Au NPs will leave the surface of UCNPs and the upconversion luminescence can be restored because of the formation of the more stable double-stranded DNA on UCNPs. The sensor we fabricated here for target DNA detection shows good sensitivity and high selectivity, which has the potential for clinical applications in the analysis of HBV and other DNA sequences.

1. Introduction

Recently, sequence-specific DNA detection has received more and more attentions due to its extreme importance in clinical molecular diagnostics of diseases, biomedical studies, microbiology and genetics.[1, 2] At present, electrochemical and also optical and gravimetric detection modes, as well as other analytical techniques have been employed for DNA detection.[3-7] Among them, fluorescence based assay offers various advantages such as high sensitivity, easy to operate and multiplexing capabilities. The fluorescent resonant energy transfer (FRET) is one of the most popular strategies in fluorescence based assays, which can provide high sensitivity and selectivity toward the target.[8-11] The FRET process occurs when (i) the emission spectra of the fluorophore (energy donor) is overlap with the absorption of the quencher (energy acceptor) and (ii) the energy donor and acceptor are close to each other, typically within 10 nm.[12] For a well-designed FRET sensor, the energy donor should provide stable fluorescent output, highly resistant to photobleaching, and the acceptor should possess high absorptivity. Meanwhile, the FRET process need to be selectively responsive to the desired target, thus the corresponding change in fluorescence intensity can be used to quantify the target concentration. [13, 14]

Upconversion nanoparticles (UCNPs) are usually composed of the oxides, fluorides, halogen oxides or other substrates as matrix and doped with trivalent rare earth ions (Er^{3+}, Eu^{3+}, Yb^{3+}, Tm^{3+}, Ho^{3+} etc.) as energy transfer system. UCNPs can convert low-energy light (NIR or IR) to higher-energy light (UV or visible) through multiple photon absorptions or energy transfer. Compared with the traditional fluorescent materials (such as organic dyes and quantum dots), UCNPs attract much more attentions due to their unique optical and chemical properties such as sharp absorption and emission bands, long lifetimes, low toxicity, superior photostability, low autofluorescence from biosamples and better tissue penetration depth.[15, 16] Therefore, UCNPs have been widely used as suitable candidates in photodynamic therapy,[17, 18] light induced drug delivery,[19] bioimaging[20] and biosensing.[21-23] In the field of fluorescence sensing, UCNPs provides two superior advantages which cannot be achieved with traditional fluorophores. First, the special luminescent mechanism (anti-Stokes luminescence) can significantly reduce autofluorescence background from the interferent and provide high signal-to-noise ratio, which leading to the high sensitivity of the UCNPs-based sensors. Second, the excellent photostability and non-blinking property of UCNPs enables them as a reliable nano-fluorophore which improves the reproducibility of the measurement.[24] All these features make UCNPs emerges as excellent energy donors in FRET system recently.

Meanwhile, gold nanoparticles (Au NPs) were widely used in all kinds of biosensors.[25] The easy surface chemistry on Au NPs makes them versatile platform to immobilize all kinds of biomolecule for specific recognition of the desired target.[26, 27] Moreover, Au NPs possess intense light absorb ability due to their surface plasmon resonance result from the collective oscillation of the conduction electrons.[28] Their extinction coefficient are normally two or three magnitudes higher than quantum dots and organic dyes.[28] Together with their larger absorption surface area and long working distance,[29] Au NPs provide excellent quenching efficiency and play an irreplaceable role as energy acceptors in FRET system. Thus, the utilize of UCNPs and Au NPs as energy donor and acceptor will lead to a series of promising aspects for FRET-based sensors, such as high photostability, high sensitivity, good reproducibility and strong expandability.

Hepatitis B virus (HBV) infection is a well-known disease for its significance as a major cause of morbidity and mortality. Accordingly, about 70% of hepatocellular carcinoma cases are developed from the chronical hepatitis type B. HBV also has a capacity to escape immune surveillance by mutations of the structural genes, which encode epitopes that are recognized by the immune system, resulting in a quasi-species population. The HBV-related death is about 500,000–700,000 every year.[30, 31] Therefore, it is urgent to improve the detection technique to prevent and control HBV infection. Although several strategies have been reported for HBV DNA detection, [32-36] there is still no report using UCNPs-based FRET assays.

Taking advantage of the unique optical properties of UCNPs and Au NPs, here we report a simple sensing platform for HBV DNA sequence determination with a FRET strategy. UCNPs and Au NPs were first connected with each other through two partially complementary single-stranded DNA, which lead to the quench of the upconversion luminescence. Upon the present of the target (HBV DNA), Au NPs will leave the surface of UCNPs and the upconversion luminescence (UCL) can be restored due to the formation of the more stable double-stranded DNA on UCNPs (Scheme 1). The fabricated sensor here exhibits good sensitivity and high selectivity, which has great potential for clinical applications in the analysis of HBV and other DNA sequences.

2. Experimental Section

2.1 Materials

All starting materials were obtained from commercial supplies and used as received. $YCl_3 \cdot 6H_2O$ (99.99%), $YbCl_3 \cdot 6H_2O$ (99.99%), $ErCl_3 \cdot 6H_2O$ (99.9%) , ethylene glycol (EG, 99%), poly(ethylenimine) (PEI, branched polymer, 25 kDa), NH_4F (98%), 2-[4-(2-Hydroxyethyl)-1-piperazinyl] ethane sulfonic acid (HEPES, ≥99.5%), glutaraldehyde (25% in H_2O) were purchased from Sigma-Aldrich. Chloroauric acid tetrahydrate ($HAuCl_4 \cdot 4H_2O$) was purchases from Sinopharm Chemical Reagent Co., Ltd. All oligonucleotides were supplied by Sangon Biotechnology Co., Ltd. (Shanghai, China). Other chemical reagents with analytical grade were used directly without further purification. Ultrapure water (Milli-Q, Millipore) was used throughout.

The sequences of oligonucleotides used in this work are as follows:

Sequence 1: 5'-NH_2-C_6-TTT GAG GAG TTG GGG GAG CAC ATT-3'

Sequence 2: 5'-SH-AAA CTC CCC CAA CTC-3'

Target DNA: 5'-AAT GTG CTC CCC CAA CTC CTC -3'

Mis 1：5'-AAT GTG CTC GGG CAA CTC CTC -3'

Mis 2：5'-CTA AGT AAC TCT GCA CTC TTT AGC CCT GAT-3'

2.2 Synthesis of PEI modified $NaYF_4$: Yb, Er (NH_2-UCNPs)

The synthesis of $NaYF_4$: 18% Yb, 2% Er nanoparticles was developed via a modified literature procedure.[37, 38] Typically, 1.2 mmol NaCl and 0.6 mmol $RECl_3$ (0.480 mmol YCl_3, 0.108 mmol $YbCl_3$ and 0.012 mmol $ErCl_3$) was added to a 100 mL flask containing 5 mL EG, 0.15 g PEI dissolved in 5 mL EG was added to the flask under stirring, then a well-agitated transparent solution of 5 mL EG charged with 0.1320 g NH_4F was added to the system. The resulting mixture was agitated for another 30 min under the room temperature before it transferred to a 50 mL of Teflon-lined autoclave, and subsequently heated to 200 °C. After 24 h hydrothermal treatment, the autoclave was cooled down to room temperature. The obtained nanoparticles were collected by centrifugation, washed with ethanol and water several times, and dried at 50 °C for 24 h.

2.3 Preparation of Au NPs

Au NPs were prepared by citrate reduction of $HAuCl_4$, based on a modified literature procedure.[39] Prior to synthesis of Au NPs, all glassware used was cleaned in aqua regia (mixture of HCl and HNO_3 with the ratio of 3:1) and rinsed thoroughly with DI water. In a typical experiment, 6.18 mL 1% HAuCl4 solution and 143.82 mL DI water were added to a round-bottom flask equipped with a reflux condenser under vigorous stirring. Then the flask was incubated into oil bath to reflux under stirring. Under the boiling solution, 15 mL 38.8 mM trisodium citrate solution was quickly added to the system, and the reaction was allowed to reflux for another 15 min after the color of the solution changed from pale yellow to deep red. Then the solution was cooled to room temperature and then stored at 4 °C for the further use.

2.4 Conjugation of NH_2-UCNPs with sequence 1

Sequence 1 was conjugated with $NaYF_4$:Yb, Er using glutaraldehyde as the cross-linking agent. 1 mg of NH_2-UCNPs was dissolved in 1 mL of HEPES (20 mM, pH 7.4), followed by adding 20 μL of glutaraldehyde (25% in H_2O) to the mixture. After shaking for reaction with an hour at room temperature, it was centrifuged and washed by the buffer for 2 times to remove excess glutaraldehyde and resuspended in 1 mL HEPES solution. Thereafter, 20 μL of sequence 1 (100 μM) was added to the activated UCNPs, and the mixture was incubated at 37 °C under gentle shaking for 12 h. NH_2-UCNPs conjugated with sequence 1 (UCNPs-seq 1) were harvested with centrifugation and washing.

Finally, the product was diluted with 1mL HEPES (20 mM, 50 mM KCl, 5 mM $MgCl_2$, pH 7.4) and stored at 4 °C for future use.

2.5 Conjugation of Au NPs with sequence 2

Sequence 2 was conjugated with Au NPs via a modified literature procedure. [40] 400 μL of as-prepared Au NPs were resuspended in 400 μL of PBS (10 mM, pH 7.4). 3 μM of sequence 2 was added to the Au NPs dispersoid, and the mixture solution was incubated at 37 °C for 24 h. Then 0.1 M of NaCl was added by drop-wise to the solution to age for 24 h. The solution was centrifuged and the remaining red oily precipitate at bottom was collected. To remove the excess sequence 2, the red precipitate was washed with PBS three times. Finally, sequence 2 conjugated with Au NPs (Au NPs-seq 2) were dispersed in 400 μL of PBS (10 mM, pH 7.4) and stored at 4 °C for future use.

2.6 Hybridization of UNCPs-seq 1 and Au NPs-seq 2

To investigate the hybridization between UCNPs-seq 1 and Au NPs-seq 2, 40 μL of as-prepared UCNPs-seq 1 and different volumes of Au NPs-seq 2 (20 μL, 40 μL, 60 μL, 80 μL, 100 μL and 120 μL) was hybridized. After adjusting the total volume to 400 μL with HEPES (20 mM, 50 mM KCl, 5 mM $MgCl_2$, pH 7.4), the system was incubated at 37 °C for an hour. The upconversion luminescence (UCL) spectra of the final mixture were recorded on a ZolixScan ZLX-UPL spectrometer with an external 980 nm laser as the excitation source.

2.7 Target DNA detection

In a typical UCNPs-based FRET assay procedure, 40 μL of as-prepared UCNPs-seq 1 and 80 μL of Au NPs-seq 2 were first hybridized, then various concentrations of target DNA were added. After adjusting the total volume to 400 μL with HEPES (20 mM, 50 mM KCl, 5 mM $MgCl_2$, pH 7.4), the system was incubated at 37 °C for an hour. The UCL spectra of the final mixture were also recorded under excitation of 980 nm. To assess the specificity of the sensor, two mismatch sequences (Mis-1 and Mis-2) were added to the system respectively following the identical procedure.

2.8 Characterization

The morphology and structure were characterized by transmission electron microscope (TEM) using a JEOL-2100 TEM operating at 200 kV. Energy-dispersive X-ray (EDX) analysis spectra were obtained by a field-emission scanning electron microscope (Hitachi S4800, Japan) equipped with an an EDAX Genesis analysis system. X-ray power diffraction (XRD) measurements were performed on a Japan Shimadzu XRD-6000 diffractometer with Cu-Ka radiation(λ = 0.15418 nm) , and a scanning rate of 0.05 deg s^{-1} was applied to record the patterns in the 2θ range of 10-80°. Zeta potential was measured on a Nano-Z Zetasizer. The UV-vis absorption and The fourier transform infrared (FT-IR) spectra were obtained using a UV-3600 spectrophotometer and a NICOLET iS10 FT-IR spectrometer, respectively. Upconversion fluorescence spectra were recorded on a ZolixScan ZLX-UPL spectrometer using an external 1 W continuous-wave laser (980 nm) as the excitation source.

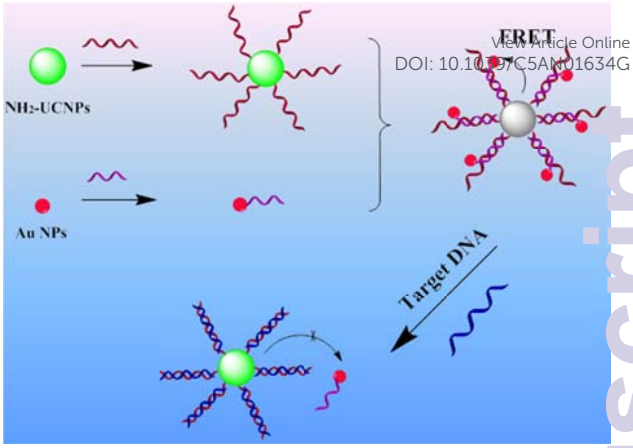

Scheme 1 Schematic illustration of the FRET biosensor for HBV DNA detection based on UCNPs.

3. Results and discussion

3.1 Principle of FRET platform for target DNA detection

As shown in Scheme 1, we developed a simple platform for H[illegible] DNA detection with $NaYF_4$: Yb, Er and Au NPs as the FRET pair. From Fig. 1, the UV-vis absorption spectrum of Au [illegible] (energy acceptor) overlaps with the fluorescence emission band of NH_2-UCNPs (energy donor) centered at 543 and 656 nm, which could be attributed to the $^4S_{3/2} \rightarrow {}^4I_{15/2}$ and $^4F_{9/2} \rightarrow {}^4I_{1[illegible]}$ transitions of Er^{3+}, respectively.[41] Here, two synthetic DNA sequences are employed in the sensor fabrication: the first or[illegible] (sequence 1) is functionalized with amino-group at the 5'-end so

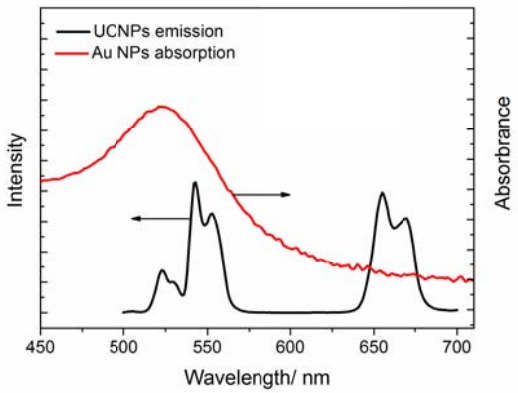

Fig. 1 The absorption (red line) spectrum of Au NPs aqueou[illegible] solution and the emission spectrum (black line) of NH_2-UCNPs .

as to bind to PEI modified $NaYF_4$: Yb, Er (NH_2-UCNPs) using glutaraldehyde as the cross-linking agent. The second one (sequence 2) is labeled with mercapto-group at the 5'-end in order to be conjugated with Au NPs. Sequence 2 is designed to b[illegible] partially complementary (12 base pairs) to sequence 1. With this arrangement, the two sequences naturally assemble to form [illegible] stable duplex state, keeping Au NPs and NH_2-UCNPs in clos[illegible] proximity with each other in the absence of target DNA. As a

result, the FRET from NH_2-UCNPs to Au NPs occurs under the excitation at 980 nm. Conversely, in the presence of HBV DNA, sequence 1-target complex structure should be preferentially formed because the target DNA has 21 complementary base pairs (9 base pairs more compare with sequence 2) with sequence 1. Consequently, the sequence 2 conjugated Au NPs will leave the surface of UCNPs, thus the UCL will be restored. Our results showed that the relative UCL intensity restore was in linear with the concentration of HBV DNA in the range of 0 ~ 50 nM. Due to the high specific recognition capability and designability of oligonucleotides, our proposed method can also be extended for the detection of a variety of DNA sequences.

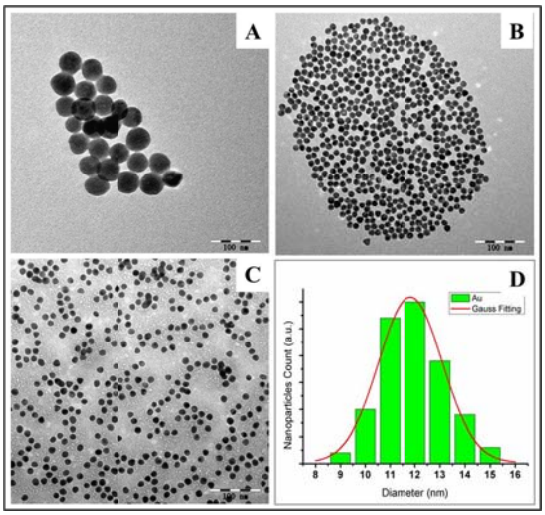

Fig. 2 TEM images of NH_2-UCNPs (A, in water), Au NPs before (B, in PBS) and after (C, in PBS) conjugated with sequence 2, as well as the histogram of particle size for Au NPs, the data was obtained from the TEM images over more than 300 upconversion nanoparticles with R-square value 0.9808 (D).

3.2 Characterization of the nanoparticles

We select $NaYF_4$:Yb,Er as the upconversion donor since it is so far the most efficient NIR-to-Visible upconversion materials due to the low phonon energy of $NaYF_4$ as the host matrix. To obtain the optimum synthesis condition, different F/Ln molar ratios were added to the hydrothermal system and the system were reacted for different times. As shown in Fig. S3 and S4, the diameters of the as-prepared NH_2-UCNPs change from 16 nm to 110 nm and the UCL intensities are enhanced sharply with the F/Ln molar ratio increasing from 4:1 to 10:1. The evolution of crystal phase from cubic phase to mixed phase with the increasing of F/Ln was also clearly observed in the corresponding XRD patterns (Fig. S5). It is well-known that hexagonal phase and larger size can lead to higher upconversion efficency, however large diameter was not favored in FRET due to the low energy transfer efficiency.[42] Therefore, the F/Ln molar ratio of 6:1 was applied in this work. The reaction time also plays an important role for the preparation of high quality NH_2-UCNPs. The diameter (Fig. S6) and crystal phase (Fig. S7) were almost unchanged when the system is reacted from 2 to 24 hours, while the UCL intensities enhanced significantly as the reaction is prolonged (Fig. S8). To obtain the most proper NH_2-UCNPs applied in this work, the F/Ln molar ratio and the reaction time are fixed to be 6:1 and 24 hours here, respectively. Fig. 2A dispalys typical TEM images of the upconversion nanoparticles after optimization. The monodispersed nanosphere of the as-prepared samples had an average size of about 48.0 nm. The TEM images also indicated that the as-prepared NH_2-UCNPs were well-dispersed in aqueous solution. XRD patterns of NH_2-UCNPs can be indexed to pure cubic phase of $NaYF_4$ (JCPDS No.77-2042) (Fig. 3A). The capping ligands on the surface of the nanoparticles were identified by FT-IR spectra (Fig. 3B). The peaks at 2940 and 2850 cm^{-1} are assigned to the asymmetric (υ_{as}) and symmetric (υ_s) stretching vibrations of methylene(-CH_2-) in PEI. The peaks at 1637 cm^{-1} and 1566 cm^{-1} can be assigned to the bending vibration of N-H. The peak at 1472 cm^{-1} resulting from the bending vibration of the C-H bond in PEI could also be found. The FT-IR result certified that NH_2-UCNPs were formed successfully.

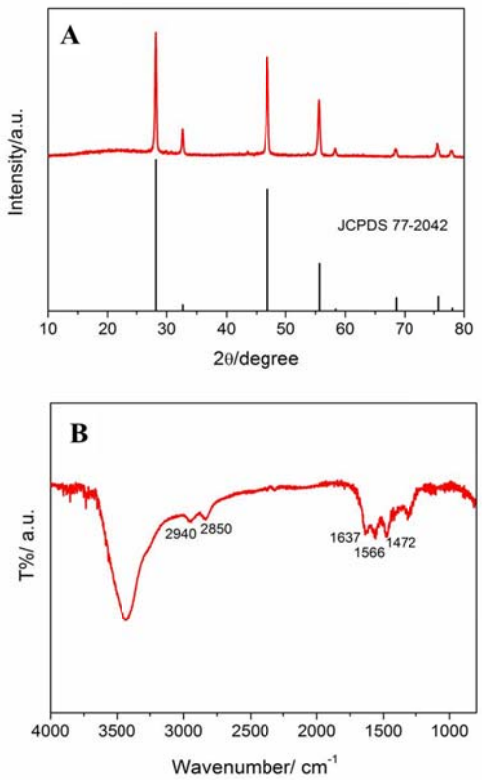

Fig. 3 XRD pattern (A) and FT-IR spectra (B) of NH_2-UCNPs.

The conjugation between sequence 1 and NH_2-UCNPs was achieved via glutaraldehyde cross-linking and was verified by the analysis of zeta potential spectroscopy and energy dispersive X-ray (EDX). The zeta potential of the nanocomposites changed from positive (+46.9 mV) to negative (-12.0 mV) after sequence 1 conjugation which was due to the negative charges carried by conjugated oligonucleotides (Fig. S1). Additionally, the chemical composition of sequence 1 conjugated with NH_2-UCNPs was also certified by energy dispersive X-ray (EDX), the EDX analysis (Fig. S2) indicates the presence of Na, Y, F, Yb, Er, O and P. The first five elements are due to presence of $NaYF_4$: Yb, Er while the

existence of O and P is evident for the successful conjugation of sequence 1 on NH_2-UCNPs (UCNPs-seq 1).

Au NPs were obtained by the citrate reduction of chloroauric acid as previous reported.[39] Fig. 2B presents a typical TEM image of the as-prepared citrate modified Au NPs, which are spherical, uniform and monodispersed. The average size of the Au NPs was calculated to be 11.9 nm (Fig. 2D). Sequence 2 was immoblized on Au NPs (Au NPs-seq 2) later through thiol chemistry. The Au NPs still exhibits good dispersed in aqueous solution and the size remain unchanged after the cojugation (Fig. 2B, C). The concentration of the Au NPs solution was estimated to be 7.4 nM according to the Lambet-Beer's law (extinction coefficient ~ 2×10^8 $M^{-1}\cdot cm^{-1}$).[43]

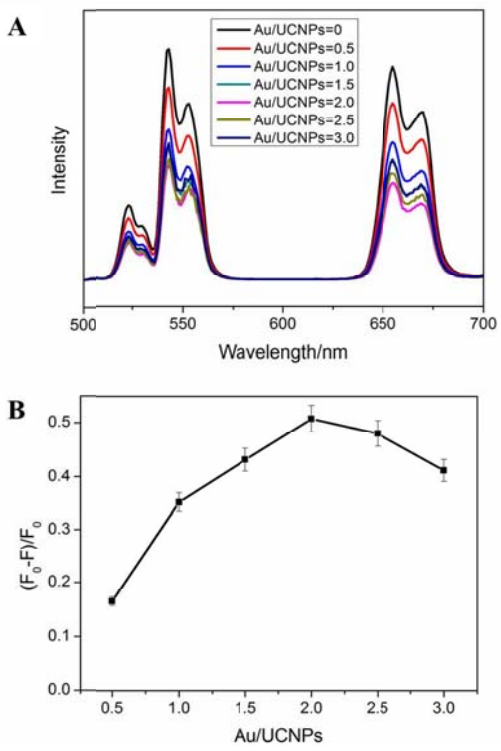

Fig. 4 UCL spectra of the UCNPs-seq 1 after hybridization with various concentrations of Au NPs-seq 2 under excitation of 980 nm (A). The effect of volume ratio of UCNPs-seq 1 to Au NPs-seq 2 on the FRET efficiency (B).

3.3 FRET between UCNPs-seq 1 and Au NPs-seq 2

In order to obtain high FRET efficiency, the excess of Au NPs-seq 2 in the solution had to be minimized. An experiment was carried out by gradually adding Au NPs-seq 2 to a solution containing UCNPs-seq 1 and the UCL spectra was measured accordingly (Fig. 4A). To quantify the FRET efficiency from the UCNPs to Au NPs, the FERT efficiency is defined as $(F_0-F)/F_0$ according to Foster's theory, where F_0 and F represent the UCL intensity of UCNPs-seq 1 at 543 nm before and after the hybridization with Au NPs-seq 2, respectively. As shown in Fig. 4B, the FRET efficiency increased with the increasing of the volume ratio of Au NPs-seq 2 to UCNPs-seq 1 when less than 2:1, and after that, the efficiency decreased when the ratio continue increasing. Similar phenomenon was also reported in the literature which use DNA modified Au NPs to quench the fluorescent of dye-doped silica nanoparticles.[44] We guess this phenomenon may be related to the formation of the assembly between UCNPs and Au NPs. Here, the FRET efficiency reached its maximum when the volume ratio of Au NPs-seq 2 to UCNPs-seq 1 was 2:1. The sucessful conjugation between UCNPs and Au NPs was also demonstrated with TEM characterization (Fig. S9). Note that although the absorbance of Au NPs at 540 nm was higher than 650 nm, the quenching efficiency was quite similar here, which was in accord with the previously report.[29]

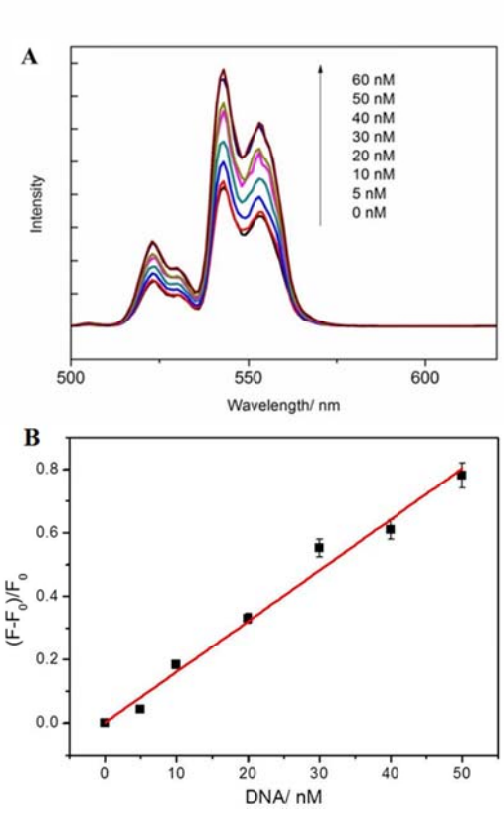

Fig. 5 UCL spectra of the sensor with various concentrations of target DNA under excitation of 980 nm (A). The linear relationship of the relative fluorescence intensity versus the concentration of HBV DNA in the range from 0 to 50 nM. F_0 and F denote the UCL intensity at 543 nm before and after addition of target DNA (B).

3.4 FRET analysis of target DNA

After the hybridization with Au NPs-seq 2, the UCL of the UCNPs-seq 1 was quenched and the formed UCNP-DNA-Au NPs nanocomposites can be used as nanoprobe for the detection of HBV DNA. When the increasing amount of target DNA was introduced into the system, the emission intensity of the UCNPs-seq 1 was restored gradually. This can be explained by the separation of the acceptor from the donor due to the better complementation of the target DNA towards sequence 1

UCNPs comparing with sequence 2. The relative fluorescence intensity was in linear with the concentration of target DNA ranging from 0 to 50 nM (Fig. 5) and the limit of the detection (LOD) of HBV DNA is as low as 250 pM, determined with the control signal plus three times of noise (standard derivation of the blank).

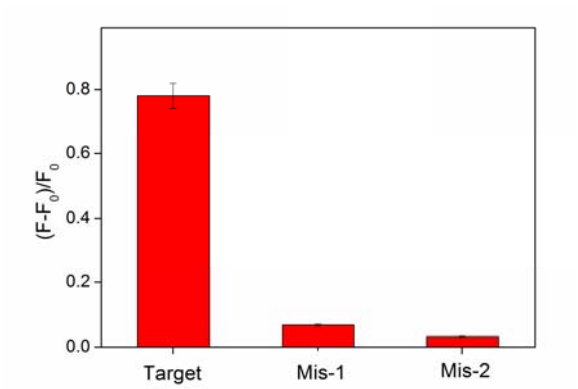

Fig. 6 Specificity of the sensor toward other sequences. The concentration of the three sequences are fixed to be 50 nM.

3.5 Specificity evaluation

To examine the specificity of the sensor for target DNA, control experiments were performed with the fixed concentration of both UCNPs-seq 1 and Au NPs-seq 2 in the presence of two mismatch sequences. The two mismatch sequences were designed to be 3-mismatching base-pairs (mis-1) and completely mismatching (mis-2) toward the sequence 1. Under identical hybridization conditions, the $(F-F_0)/F_0$ was determined, where F_0 represents the UCL intensity at 543 nm of the mixture of UCNPs-seq 1 and Au NPs-2, and F represents the intensity after the addition of target DNA or the mismatch sequences. As shown in Fig. 6, obvious response was observed when target DNA was introduced to the assay system, whereas the non-specific sequences, especially mis-2 gave little response. These results indicate the high selectivity of the proposed method.

4. Conclusions

Taking advantages of the unique optical properties of UCNPs and Au NPs, we have constructed a novel upconversion FRET sensing platform for the determination of HBV DNA sequence. The energy transfer between NH_2-UCNPs and Au NPs occurs, when they were conjugated with two partly complementary oligonucleotide sequences and mixed together. However, in the presence of target DNA, the upconversion luminescence recovery was observed, and the relative recovery intensity was proportional to the concentration of the target. This method is fairly simple, convenient and shows good sensitivity as well as high selectivity, which has great potential for clinical applications in the analysis of HBV and other DNA sequences.

Acknowledgements

We greatly appreciate the financial support from National Natural Science Foundation of China (NSFC) (21175071, 21335004) and the support from 973 Program (No. 2011CB933502).

Notes and references

State Key Laboratory of Analytical Chemistry for Life Science, Collaborative Innovation Center of Chemistry for Life Science, School of Chemistry and Chemical Engineering, Nanjing University, Nanjing, 210093, P. R. China. Fax: 86-25-83597204; Tel: 86-25-83597204; E-mail: wuxingca@nju.edu.cn, jjzhu@nju.edu.cn

† Electronic Supplementary Information (ESI) available: [details of any supplementary information available should be included here]. See DOI: 10.1039/b000000x/

‡These authors contributed equally to this work.

1. L. Hood and D. Galas, *Nature*, 2003, **421**, 444-448.
2. J. Zhang, H. G. Nie, Z. Wu, Z. Yang, L. J. Zhang, X. J. Xu and S. M. Huang, *Anal. Chem.* , 2014, **86**, 1178-1185.
3. C. S. Wu, T. Bronder, A. Poghossian, C. F. Werner, M. Backer and M. J. Schoning, *Physica Status Solidi a-Applications and Materials Science*, 2014, **211**, 1423-1428.
4. S. S. Zhang, H. Zhong and C. F. Ding, *Anal. Chem.* , 2008, **80**, 7206-7212.
5. B. J. Zou, X. M. Cao, H. P. Wu, Q. X. Song, J. P. Wang, T. Kajiyama, H. Kambara and G. H. Zhou, *Biosensors & Bioelectronics*, 2015, **66**, 50-54.
6. J. Chen, H. D. Qiu, M. L. Zhang, T. N. Gu, S. J. Shao, Y. Huang and S. L. Zhao, *Biosensors & Bioelectronics*, 2015, **68**, 550-555.
7. H. Y. Huang, W. Q. Bai, C. X. Dong, R. Guo and Z. H. Liu, *Biosensors & Bioelectronics*, 2015, **68**, 442-446.
8. D. Dey, J. Saha, A. D. Roy, D. Bhattacharjee, S. Sinha, P. K. Paul, S. Chakraborty and S. A. Hussain, *Sensors and Actuators B-Chemical*, 2014, **204**, 746-753.
9. G. L. Wang, H. Q. Luo and N. B. Li, *Analyst*, 2014, **139**, 4572-4577.
10. H. A. Al Attar and A. P. Monkman, *Adv. Funct. Mater.* , 2008, **18**, 2498-2509.
11. R. Y. Zhou, C. Xu, J. Dong and G. J. Wang, *Biosensors & Bioelectronics*, 2015, **65**, 103-107.
12. D. J. Maxwell, J. R. Taylor and S. M. Nie, *J. Am. Chem. Soc.* , 2002, **124**, 9606-9612.
13. A. H. Erbse, A. J. Berlinberg, C. Y. Cheung, W. Y. Leung and J. J. Falke, *Biochemistry*, 2011, **50**, 451-457.
14. Y. Wang, Z. Wu and Z. Liu, *Anal. Chem.* , 2013, **85**, 258-264.
15. F. Wang and X. G. Liu, *Chem. Soc. Rev.* , 2009, **38**, 976-989.
16. M. Haase and H. Schafer, *Angew Chem Int Edit*, 2011, **50**, 5808-5829.
17. L. Xia, X. G. Kong, X. M. Liu, L. P. Tu, Y. L. Zhang, Y. L. Chang, Y. Liu, D. Z. Shen, H. Y. Zhao and H. Zhang, *Biomaterials*, 2014, **35**, 4146-4156.
18. C. Wang, L. Cheng, Y. M. Liu, X. J. Wang, X. X. Ma, Z. Y. Deng, Y. G. Li and Z. Liu, *Adv. Funct. Mater.* , 2013, **23**, 3077-3086.
19. Y. L. Dai, H. H. Xiao, J. H. Liu, Q. H. Yuan, P. A. Ma, D. M. Yang, C. X. Li, Z. Y. Cheng, Z. Y. Hou, P. P. Yang and J. Lin, *J. Am. Chem. Soc.* , 2013, **135**, 18920-18929.
20. Y. J. Ding, H. Zhu, X. X. Zhang, J. G. Gao, E. S. Abdel-Halim, L. P. Jiang and J. J. Zhu, *Nanoscale*, 2014, **6**, 14792-14798.
21. Z. G. Chen, H. L. Chen, H. Hu, M. X. Yu, F. Y. Li, Q. Zhang, Z. G. Zhou, T. Yi and C. H. Huang, *J. Am. Chem. Soc.* , 2008, **130**, 3023-3029.
22. S. Wu, N. Duan, X. Ma, Y. Xia, H. Wang, Z. Wang and Q. Zhang, *Anal. Chem.* , 2012, **84**, 6263-6270.
23. H. Zhu, Y. Ding, A. Wang, X. Sun, X.-C. Wu and J.-J. Zhu, *J. Mater. Chem. B*, 2015, **3**, 458-464.
24. X. G. Liu, C. H. Yan and J. A. Capobianco, *Chem. Soc. Rev.* , 2015, **44**, 1299-1301.
25. F. Lu, T. L. Doane, J. J. Zhu and C. Burda, *Inorg. Chim. Acta* 2012, **393**, 142-153.

26. J. Li, S. P. Song, X. F. Liu, L. H. Wang, D. Pan, Q. Huang, Y. Zhao and C. H. Fan, *Adv. Mater.* , 2008, **20**, 497-500.
27. G. P. Acuna, M. Bucher, I. H. Stein, C. Steinhauer, A. Kuzyk, P. Holzmeister, R. Schreiber, A. Moroz, F. D. Stefani, T. Liedl, F. C. Simmel and P. Tinnefeld, *Acs Nano*, 2012, **6**, 3189-3195.
28. K. Saha, S. S. Agasti, C. Kim, X. N. Li and V. M. Rotello, *Chem. Rev.* , 2012, **112**, 2739-2779.
29. W. W. Ye, M. K. Tsang, X. Liu, M. Yang and J. H. Hao, *Small*, 2014, **10**, 2390-2397.
30. J. Kim, K. C. Han, Y. G. Yu and E. G. Yang, *Biochip Journal*, 2007, **1**, 134-139.
31. C. W. Shepard, E. P. Simard, L. Finelli, A. E. Flore and B. P. Bell, *Epidemiologic Reviews*, 2006, **28**, 112-125.
32. T. L. Chuang, S. C. Wei, S. Y. Lee and C. W. Lin, *Biosens. Bioelectron.* , 2012, **32**, 89-95.
33. B. H. Cha, S. M. Lee, J. C. Park, K. S. Hwang, S. K. Kim, Y. S. Lee, B. K. Ju and T. S. Kim, *Biosens. Bioelectron.* , 2009, **25**, 130-135.
34. C. Ding, F. Zhao, M. Zhang and S. Zhang, *Bioelectrochemistry*, 2008, **72**, 28-33.
35. C.-W. Huang, H.-T. Hsueh, Y.-J. Huang, H.-H. Liao, H.-H. Tsai, Y.-Z. Juang, T.-H. Lin, S.-S. Lu and C.-T. Lin, *Sens. Actuators, B* 2013, **181**, 867-873.
36. D. S. Xiang, K. Zhai, W. J. Xiang and L. Z. Wang, *Talanta*, 2014, **129**, 249-253.
37. F. Wang and X. G. Liu, *J. Am. Chem. Soc.* , 2008, **130**, 5642-5643.
38. F. Wang, D. K. Chatterjee, Z. Li, Y. Zhang, X. Fan and M. Wang, *Nanotechnology*, 2006, **17**, 5786-5791.
39. G. Frens, *Nature-Physical Science*, 1973, **241**, 20-22.
40. J. Liu and Y. Lu, *Nat. Protoc.* , 2006, **1**, 246-252.
41. Y. H. Zhang, L. X. Zhang, R. R. Deng, J. Tian, Y. Zong, D. Y. Jin and X. G. Liu, *J. Am. Chem. Soc.* , 2014, **136**, 4893-4896.
42. Z. Li, S. W. Lv, Y. L. Wang, S. Y. Chen and Z. H. Liu, *J. Am. Chem. Soc.* , 2015, **137**, 3421-3427.
43. Y. B. Zu and Z. Q. Gao, *Anal. Chem.* , 2009, **81**, 8523-8528.
44. F. Gao, P. Cui, X. X. Chen, Q. Q. Ye, M. G. Li and L. Wang, *Analyst*, 2011, **136**, 3973-3980.

View Article Online
DOI: 10.1039/C5AN01634G